Formation of Organic Nanoscale Laminates and Blends by Molecular Layer Deposition

Paul W. Loscutoff,[†] Han Zhou,[‡] Scott B. Clendenning,[§] and Stacey F. Bent[†,*]

[†]Department of Chemical Engineering, Stanford University, [‡]Department of Chemistry, Stanford University, and [§]Intel Corporation, Hillsboro, Oregon

ABSTRACT Nanoscale organic films are important for many applications. We report on a system of molecular layer deposition that allows for the deposition of conformal organic films with thickness and composition control at the subnanometer length scale. Nanoscale polyurea films are grown on silica substrates in a layer-by-layer fashion by dosing 1,4-phenylene diisocyanate (PDIC) and ethylenediamine (ED) in the gas phase. Ellipsometry measurements indicate that the film growth occurs at a constant growth rate, with film thicknesses consistent with molecular distances calculated using density functional theory. Characterization of the films by Fourier transform infrared spectroscopy and X-ray photoelectron spectroscopy reveals formation of stable polyurea films with nearly stoichiometric composition, and transmission electron microscopy indicates that the films uniformly coat the substrate surface. Subnanometer control over the film composition was demonstrated using 2,2′-thiobis(ethylamine) (TBEA) as an alternate diamine to vary the composition of the films. By substituting TBEA for ED, blended films, with homogeneous composition through the film, and nanolaminates, with discrete layers of differing film chemistry, were created.

KEYWORDS: molecular layer deposition · laminate · chemical vapor deposition · surface · thin film · organic · coating

Nanoscale organic films have gained increased interest in recent years, due to the shrinking dimensions of electronic devices. Increasingly, organic films are finding application as key components in devices traditionally dominated by conventional inorganic films. From the advent of organic electronics, the importance of nanoscale organic films has become evident. For example, covalently bound organic self-assembled monolayers have been employed as interfacial layers between substrates and organic semiconductors to aid in film ordering,[1−4] and also used as the organic semiconductor layer, in organic thin film transistors.[5,6] Organic films are also used in chemical sensors,[7] and as wires and dielectrics in molecular electronics.[8−10] Recently, interest has grown in using nanoscale organic films to replace more conventional materials in silicon-based electronics as approaching atomic dimensions puts severe limitations on materials properties. Already, organic films have shown promise as copper diffusion barriers and liners for interconnect processing,[11−15] and it is likely that nanoscale organic films will receive more attention in the future as alternatives to current photoresists as lithography exposure wavelengths are pushed smaller and smaller.

Molecular layer deposition (MLD) is an emerging film growth technique that is capable of depositing nanoscale organic films. Analogous to atomic layer deposition (ALD), which utilizes a series of self-saturating reactions between vapor phase precursors and a solid surface to create films in a layer-by-layer fashion,[16] MLD makes use of self-limiting reactions between multifunctional organic molecules to grow organic films layer by layer. While there are many organic coupling reactions that occur readily in solution, vacuum conditions impose limitations on the type and number of organic coupling reactions available for MLD. For example, the solvent is no longer available to mediate proton transfer or stabilize intermediates. Moreover, changing the pH of the solution is not an option, and using a catalyst becomes nontrivial. Thus the defining characteristic of an MLD system is the coupling chemistry. A few MLD systems have been reported to date, including reaction of dianhydrides with diamines to form polyimides,[17−19] reaction of di(acid chlorides) with diamines to form polyamides,[20−22] and reaction of diisocyanates and diamines to form polyureas[23,24] among others.[25−27] Additionally, several hybrid MLD films, using a combination of organic and inorganic precursors, have been investigated in recent years.[25,28−31]

Use of MLD for growth of organic films has many advantages over the traditional

*Address correspondence to sbent@stanford.edu.

Received for review August 14, 2009 and accepted November 30, 2009.

Published online December 11, 2009.
10.1021/nn901013r

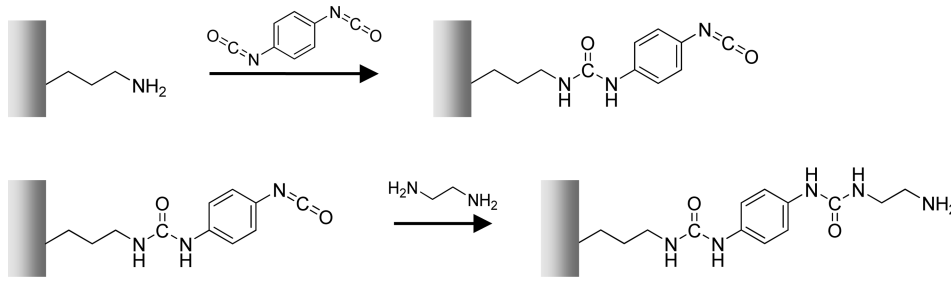

Scheme 1. MLD reaction using PDIC and ED, from an initial surface-bound amine.

chemical vapor deposition (CVD) methods. By utilizing self-limiting reactions in a binary fashion, the film thickness can be precisely controlled down to single-molecule dimensions. As the self-limiting reactions are allowed to proceed to saturation, all accessible reactive surface moieties are consumed, resulting in a complete reaction. Hence, another advantage of MLD is that the surface saturation at each step allows for conformal coating of a surface and the morphology that might be present, including high-aspect ratio features. This ability to coat surface features conformally is a general property of the MLD[25] and ALD[16] techniques, although conformal coating has been achieved with some CVD systems as well.[32−36] MLD also allows an unprecedented level of control over the composition of the deposited ultrathin organic films. In principle, the organic backbone of each monomer can be changed to tailor material properties such as chemical functionality, thermal stability, adhesion, and optical and electrical properties. Specific concentrations of alkyl, alkenyl, aryl, and heteroatom functionalities can be inserted into the film as desired, simply by using the appropriate multifunctional monomers.

In this study, we report on an MLD coupling chemistry which is very versatile: it takes place at room temperature, it produces very stable organic thin films, and it allows for a range of substitutions in the backbone. This in turn enables composition control in the films at the subnanometer scale, as we demonstrate by the production of 100 nm thick nanolaminates and blends. In particular, we describe the room temperature growth of polyurea films by MLD using an isocyanate−amine urea coupling reaction. Traditional CVD of polyurea films has been thoroughly studied, owing to the interesting polyurea film properties including piezoelectricity,[37−41] pyroelectricity,[42] and ferroelectricity.[41,43] The urea coupling reaction proceeds without any byproduct, eliminating the need for a film-curing anneal to complete reaction, as is the case with polyimides,[17−19] and avoiding byproduct entrapment or reaction with the polymer film, as is observed with polyamide formation.[21] Additionally, the linear growth observed for small cycle numbers continues past 75 cycles, without a reduction of the growth rate at higher cycle number as has been observed in other MLD systems.[27] By adding a second diamine into the MLD sequence, we demonstrate control over film composition, creating homogeneous "blended" films using repeating supercycles, i.e. combinations of varying numbers of single diisocyanate/diamine cycles. In addition to these homogeneous films, we show the ability to create nanolaminate organic films, with chemically distinct, alternating layers. This ability to precisely deposit desired functionalities within organic films is a distinct advantage of MLD, and allows for films to be tailored to specific applications by insertion of desired properties in layers from dimensions of tens of nanometers down to single molecule thickness, creating truly nanoscale organic films.

RESULTS AND DISCUSSION

Our base method for depositing polyurea films by MLD involves dosing 1,4-phenylene diisocyanate (PDIC) and ethylenediamine (ED) in an alternating sequence to build films layer-by-layer to the desired thickness. Starting from an amine-terminated surface, the MLD reaction proceeds as shown in Scheme 1. As demonstrated in the schematic, the amine-terminated surface is reacted with 1,4-phenylene diisocyanate to yield an isocyanate-terminated surface. This is then reacted with ethylenediamine, which results in an amine-terminated surface. These two steps comprise a single binary cycle. MLD is carried out by repeating these two reactions in sequence for a desired number of cycles.

Density functional theory (DFT) calculations were performed to calculate the geometry of the initial urea coupling product at the surface. While DFT is ill-suited for capturing all of the molecular interactions of self-assembled monolayers or multilayers, by building a chain off of a single molecule of 3-aminopropylsiloxane, it is possible to examine the chain angles and molecular angles of the PDIC/ED system. These angles can in turn be used to estimate the approximate thickness of layers in the film and are given in Figure 1. The calculations show that the binary cycle of PDIC and ED results in a mostly planar product projecting from the surface, since the lowest energy configuration for the urea couplings consists of the amide groups in the same plane as the phenyl ring. This planarity is favorable owing to the resonance stabilization of the molecule from π-bond delocalization of the phenyl ring to the urea groups. In this geometry, the molecular chain length is

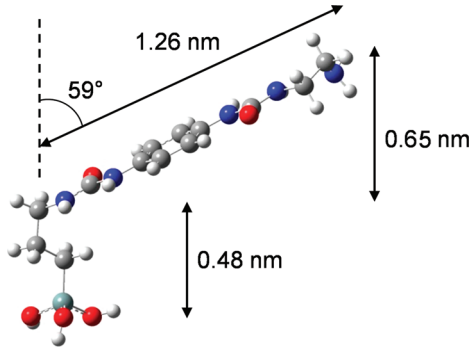

Figure 1. Optimized geometry of the product of a hydrolyzed APTES chain reacting with PDIC and subsequently ED.

1.26 nm per PDIC/ED unit. However, with the APTES extending normal to the surface, the planar portion of the surface product is tilted at an angle of 59° from the surface normal, reducing the expected thickness of a binary cycle to 0.65 nm. Although the APTES orientation may not be perfectly normal to the surface, we can expect growth rates closer to 0.65 nm/cycle than 1.26 nm/cycle.

To prepare the piranha-cleaned silicon dioxide substrates for MLD, vapor deposition of 3-aminopropyltriethoxysilane (APTES) was carried out to yield an amine-terminated surface. APTES is known to react with hydroxylated silicon oxide surfaces *via* the silanization reaction of the ethoxy groups with the surface hydroxyls, forming covalent siloxane bonds to the surface. There has been a substantial volume of work with APTES functionalization of silica surfaces, with varied results in the thickness and uniformity of the APTES surface layer.[44−51] The method employed in this study was modified from that of Zheng and Frank,[52] which produced a uniform monolayer-thick coating of APTES, with a thickness of 0.7 nm as measured by ellipsometry. While the value is larger than the calculated value of 0.48 nm (Figure 1), the experimental value agrees with the previous experimental results and is indicative of a film with monolayer thickness.[50] Moreover, the APTES surface coverage can be calculated from X-ray photoelectron spectra, and the experimental value of 6 ± 1 molecules/nm^2 agrees well with literature values of 5.3 and 6.4 molecules/nm^2 for an APTES monolayer.[53]

Following pretreatment with APTES, films of different thicknesses were deposited by carrying out various numbers of MLD cycles. The results indicate that the polyurea films were successfully grown *via* the MLD process, using PDIC and ED. Figure 2a shows the film thickness, as measured by ellipsometry, as a function of number of cycles. The data in Figure 2a shows that the reaction proceeds with a constant growth rate of 0.41 nm/cycle. Unlike many ALD processes,[16] the MLD growth studied here does not show an incubation period during which the initial growth rate is low, and instead a linear dependence of thickness on cycle number is observed from the first binary cycle.[54] The measured

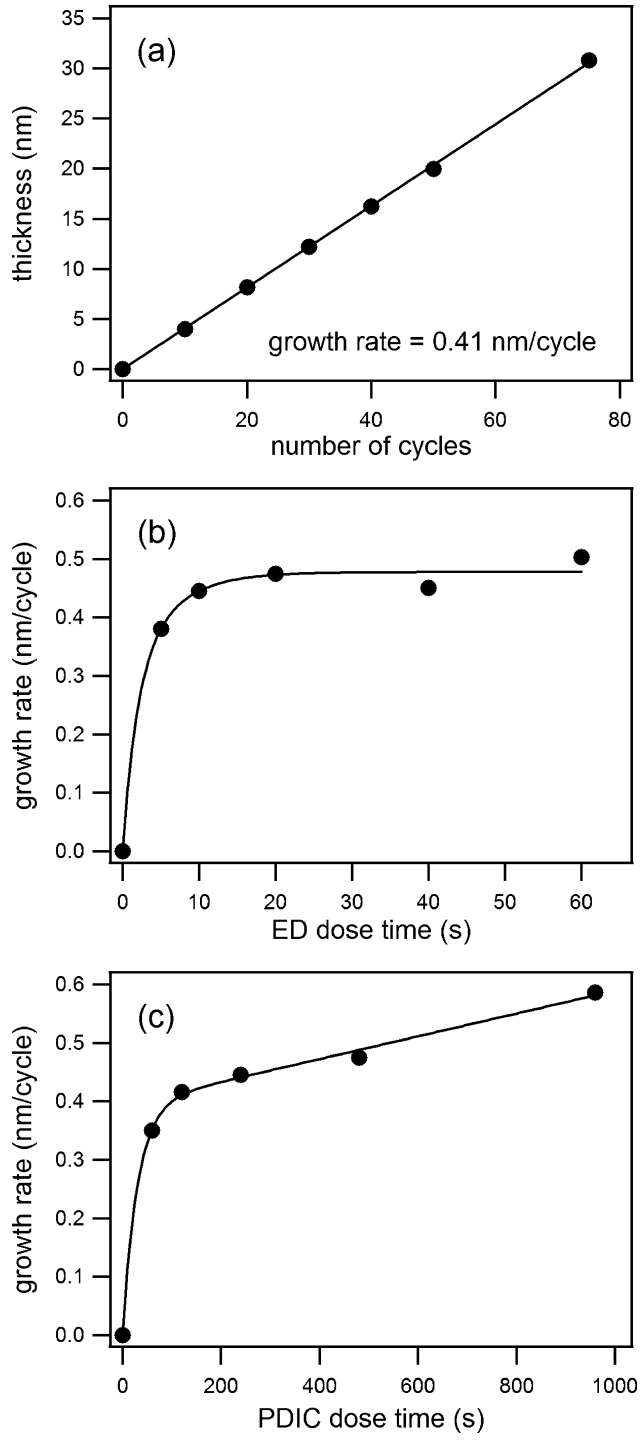

Figure 2. (a) Plot of MLD film thickness as a function of number of cycles. Saturation curves showing growth rate as a function of (b) ED dose time (PDIC dose time fixed at 240 s) (c) PDIC dose time (ED dose time fixed at 10 s).

growth rate falls within the range expected by DFT calculations, although the relatively low value indicates either that the chains are growing at an average angle of 71° from the surface normal or that the deposition occurs with subsaturation coverage per cycle, a behavior commonly observed in ALD.[16] This subsaturation growth may occur by the mechanism of island formation, in which a dense, uniform film is achieved upon

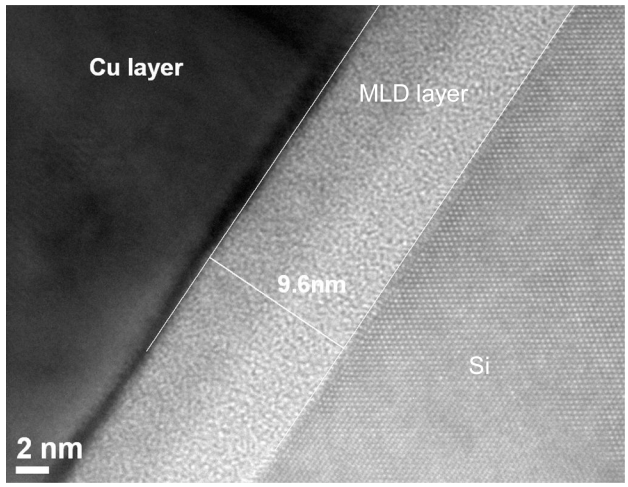

Figure 3. TEM image of 15 MLD cycle sample with evaporated Cu coating on top of the organic film.[55]

coalescence of the islands. Another possible mechanism by which subsaturation growth would result in a dense, uniform film is if monomers may react with buried sites in the film, as has been suggested for CVD growth of parylene films under certain conditions.[32,33] Importantly, we do not observe a deviation from linearity even after as many as 75 cycles, with highly repeatable growth rates, indicating that the film growth does not begin to fall off due to a double-reaction capping of the active sites, as has been proposed and observed for other MLD systems.[20,21,27,28,30]

Linear growth alone does not prove that the growth mechanism is MLD. A requirement of MLD is that the precursors react at the surface in a self-limiting manner. To test the saturation characteristics of the polyurea MLD films, the dose time of PDIC and ED were varied separately, with all other parameters held constant. For the saturation studies, 20 binary cycles of PDIC/ED were deposited in each case. To collect the data point for a pulse time of zero, the counter-monomer was dosed with normal purge times, while the monomer of interest was not dosed. In this MLD system, the ED dose times are much shorter than the PDIC dose times due to the vapor pressure of the reactants, with the vapor pressure of ED significantly higher than that of PDIC.

Over the pulse times measured, the thickness curves in Figure 2b,c show that both PDIC and ED exhibit a degree of saturation behavior. The shape of the saturation curves is typical for ALD and MLD systems, with a rapid thickness increase at low doses, and a region of slower growth or no growth at longer pulse times. The deviation from true saturation for PDIC may be due to a CVD component of the reaction, resulting from the need for longer purge times at the extended doses. Indeed, when doubling the purge time for the 960 s PDIC dose, the growth rate drops to 0.46 nm/cycle. This saturation in monomer dose time rules out condensation of the monomers on the surface and indicates that adsorption of each monomer is occurring through a limited number of active surface sites.

To complement the ellipsometry measurements of film thickness and to test the uniformity of MLD films, transmission electron microscopy (TEM) was used to visualize the cross-section of a 15 binary cycle MLD film. The TEM image is given in Figure 3. In the image, there is a lighter color band present between the silicon substrate and the Cu coating, which is attributed to the organic film. While the differences between the oxide and MLD film cannot be resolved at this resolution, the thickness of this combined SiO_2 and MLD layer is 9.6 nm and matches closely the combined film thickness measured by ellipsometry. The TEM image shows excellent film coverage and uniformity, and the lack of voids and film delamination for the MLD layer indicates good interface quality.

Transmission Fourier transform infrared (FTIR) spectroscopy was used to investigate the chemical bonding in the film to confirm that a polyurea film was deposited. Figure 4 compares the IR spectra for MLD films with different numbers of total cycles and a DFT-calculated spectrum of the expected product. The spectrum calculated by DFT is for the repeating unit of the polyurea oligiomer, which would be formed by a single binary cycle of MLD. The calculation is restricted to this single unit for computational practicality. The peak assignments are given in Table 1. Of these, the characteristic peaks created by the urea coupling are the amide I and amide II modes, at 1651 and 1510 cm^{-1}, respectively. Comparing the experimental spectra, there is a significant increase in the absorbance of the modes related to the organic film with increasing number of cycles. The films are all amine-terminated (all MLD cycles ended with an ED dose), thus no isocyanate peaks are expected, and the lack of the very strong isocyanate stretch in the range of 2000−2200 cm^{-1} indicates that there are no unreacted isocyanate groups present in the film. In other words, the PDIC has completely reacted to form urea bonds.

Comparing the theoretical spectrum to the experimental MLD spectra, it is clear that there is excellent agreement between the two. One notable difference between the experimental and calculated spectra is the amide I mode, which is at 1651 cm^{-1} in the experimental spectrum and at 1682 cm^{-1} in the calculated spectrum. This shift in the experimental spectrum results from hydrogen bonding in the film between adjacent polyurea chains. The inset of Figure 4 shows an example of the geometric structure in which hydrogen bonding can take place between the amide N−H groups and the carbonyl oxygen of the adjacent chain. This hydrogen bonding results in a red-shifting of the stretching modes for these two groups, and has been observed in previous work with polyurea films.[56] Thus, the sharp ν(C═O) peak at 1651 cm^{-1} in the experimental spectrum results from well-ordered hydrogen-bonded poly-

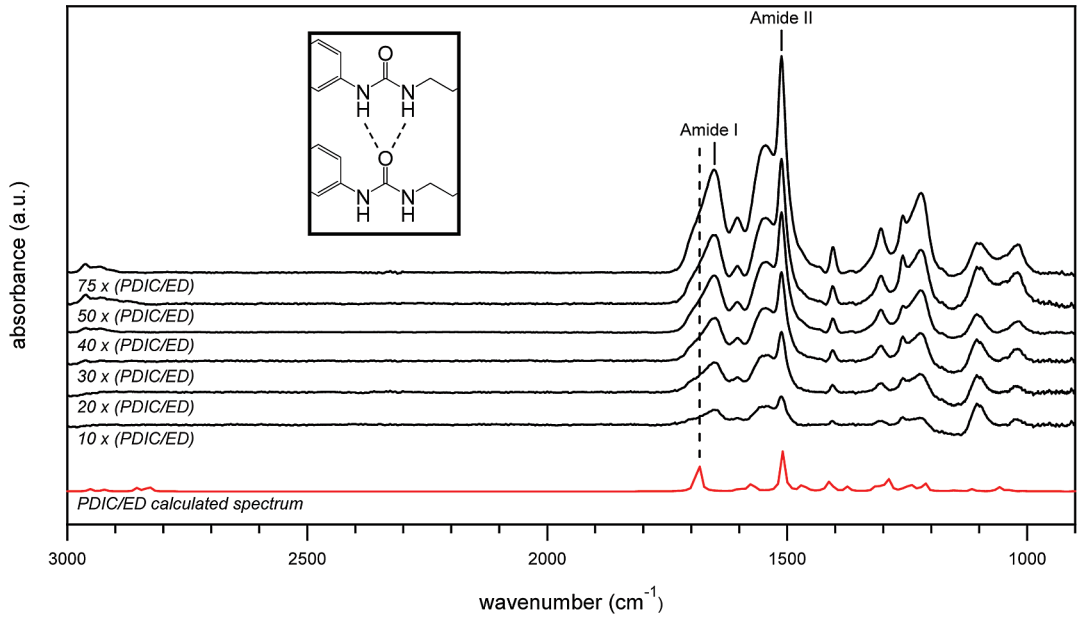

Figure 4. FTIR spectra of MLD films of different total PDIC/ED cycles and an IR spectrum calculated using DFT. Inset shows schematic of hydrogen bonding between adjacent organic chains.

urea chains. In addition to this peak, there is a shoulder extending to the blue, resulting from various levels of ordering and hydrogen bonding within the film, out to ~1710 cm^{-1} corresponding to "free" carbonyl oxygens, which are from chains not experiencing any hydrogen bonding. The effects of the hydrogen bonding are also observed in the ν(N−H) modes, which appear in the experimental spectra as a broad peak in the range 3250−3450 cm^{-1}. This N−H stretching region was not shown, owing to a high level of noise in the spectra.

To test the atomic composition of the MLD film, XPS spectra were taken of a 12 MLD cycle sample; the results are given in Figure 5. An XPS spectrum of the APTES-functionized surface is also provided for comparison. On the basis of the atomic percentages determined from XPS, the measured ratios of elements are stoichiometric within error. For an ideal film of PDIC/ED, the atomic ratios should be 5:2:1 for C/N/O. In the 12 cycle film, the atomic ratios are 4.9:1.5:1. The minor difference from the ideal ratio results from a small amount of oxygen signal due to the underlying SiO_2, and a small amount of adventitious carbon, as the only expected source of nitrogen is from the deposited organic layer.

Elemental fine scans (Figure 6) indicate the atomic environment, and are dependent on the bonding in the film. The N(1s) fine scan reveals that there is a single peak at 399.8 eV, indicative of a single type of nitrogen in the film, as expected. The O(1s) fine scan contains two separate peaks—a major peak at 531.3 eV from the carbonyl in the film, and a small peak at 533.2 eV from the underlying SiO_2 substrate. The C(1s) fine scan is the

TABLE 1. Mode Assignments for Infrared Spectra of 12 MLD Cycle Film

infrared peak assignments	
frequency (cm^{-1})	**mode**
3450−3250	ν(N−H)
3050−2850	ν(C−H)
1651	ν(C═O) amide I
1608	$\delta(NH_2)$ scissor
1556	ν(C−C) ring mode
1510	δ(N−H) amide II
1471	$\delta(CH_2)$ scissor
1404	δ(NH) + $\delta(CH_2)$ wag
1373, 1325	$\delta(CH_2)$ wag
1306	ν(C−C) ring mode + $\delta(CH_2)$ twist
1257	$\delta(CH_2)$ rock
1221	$\nu(C_{ar}\text{-}N)$ + δ(N−H)
1140	δ(C−H) ring scissoring mode
1097	ν(C−N)
1084	ν(Si−OH)
1022	ν(C−C)

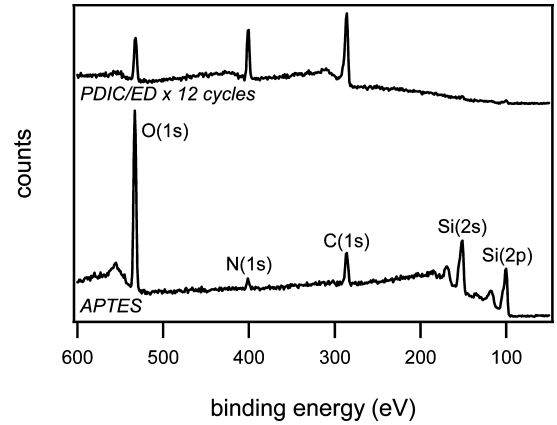

Figure 5. X-ray photoelectron spectra of survey scans for APTES film and 12 cycle PDIC/ED MLD film.

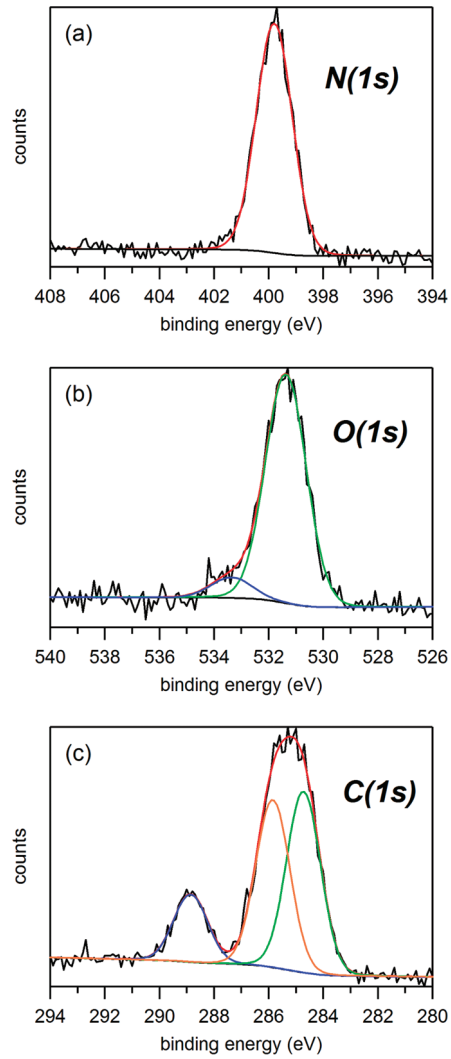

Figure 6. X-ray photoelectron spectra for fine scans of 12 MLD cycle films: (a) N (1s), (b) O (1s), (c) C (1s).

most interesting, as there are multiple types of carbons in the polyurea film, and multiple peaks are expected. Indeed, at least three distinct peaks are detected in the spectrum, as seen in Figure 6. Since binding energy increases with decreasing electron density, we expect that the peak at 284.7 eV results from the electron-rich aromatic carbons in the film. The intermediate peak at 285.9 eV is attributed to alkyl carbons, and the highest binding energy peak at 288.9 eV is due to the carbonyl carbons in the urea linkage. The theoretical ratio of these carbon types is 3:1:1 for aromatic/alkyl/carbonyl, and the experimental ratios is 2.7:2.5:1. The discrepancy between the theoretical and experimental ratios is likely due to the urea groups being attached directly to the aromatic ring. While we have assumed in the theoretical ratio that all of the aromatic carbons were approximately the same, in fact, while the four nonsubstituted aromatic carbons are identical, the substituted carbons are chemically shifted by the urea toward higher binding energy, which would lead to the expected peak ratio to be 2:2:1 rather than 3:1:1.

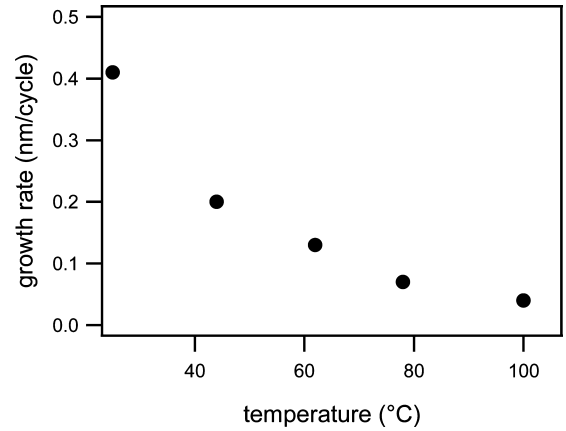

Figure 7. MLD growth rate for PDIC/ED system as a function of temperature.

The excess carbon for the aromatic and aliphatic peaks is attributed to adventitious carbon, as a vacuum break is necessary for the *ex situ* XPS analysis. The presence of the high binding energy carbonyl carbon offers further confirmation to the IR spectra that the PDIC and ED undergo urea coupling, and that the deposited film is a polyurea film, closely matching the stoichiometric atomic composition.

To test the dependence of the MLD process on temperature, the growth rate was measured at temperatures of 25, 44, 62, 78, and 100 °C, using the same precursor dose times found for saturation at 25 °C, and the results are given in Figure 7. As seen in the figure, the growth rate decreases with increasing temperature from a rate of 0.41 nm/cycle at 25 °C to just 0.04 nm/cycle at 100 °C. Although these growth rates may not represent saturation growth rates at the temperatures above 25 °C, this behavior of decreasing growth rate with increasing temperature has been observed previously for other MLD systems as well as for CVD of polyurea films and has been attributed to a precursor-mediated reaction.[20,21,38,39] A potential precursor state of the reacting molecule with the surface is a hydrogen bonding interaction. The amine hydrogens may associate with the oxygen or nitrogen of the isocyanate *via* a hydrogen bond,[57] lending stability to the reaction intermediate. With several possibilities for hydrogen bonding, the reacting molecule may sample the surface multiple times before it finds the right geometry to traverse the reaction pathway. At higher temperatures, the lifetime of such hydrogen-bonded species would be diminished, reducing the growth rate.

The polyurea films deposited by MLD demonstrated excellent stability when exposed to both atmospheric conditions and elevated temperature. Upon exposure to lab ambient for 2 weeks, the polyurea films showed negligible change in film thickness and chemical composition. Additionally, the films are stable to a temperature of at least 250 °C when annealing under vacuum, as indicated by the minimal changes observed in the FTIR spectra.[58]

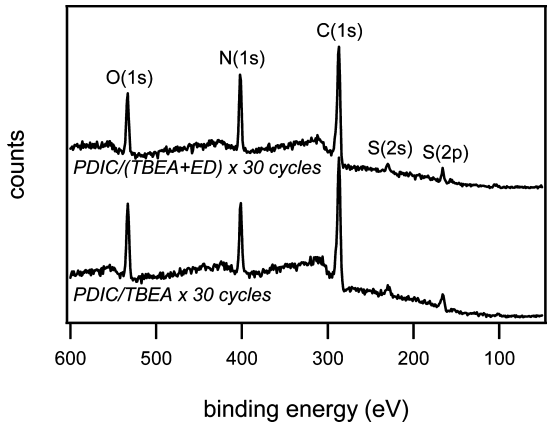

Figure 8. XPS spectra for MLD films with 30 cycles of PDIC/ED and PDIC/(ED+TBEA).

One of the strengths of the urea coupling chemistry is that it allows for substitutions within the precursor backbone without significantly altering the kinetics of the coupling reaction or interfering with the MLD process. Some examples of backbone modification are the addition of a sulfide group and substitution of the alkyl chain for an aryl group in the diamine. By using these molecules in place of ethylenediamine in the MLD scheme, the film composition can be varied as desired. Similar changes can be made to the diisocyanate backbone. Moreover, both blended films (with constant composition through the film) and laminates (with a sequence of discrete layers) can be deposited by MLD. These laminate films allow for a wide range of geometries, with layers of thicknesses from tens of nanometers to less than a single nanometer possible.

To demonstrate this capability, MLD studies using 2,2′-thiobis(ethylamine) (TBEA) were conducted and analyzed using XPS sputter depth profiling. TBEA contains a sulfide group within the diamine backbone. In these experiments, ED cycles were replaced with TBEA cycles, always leaving PDIC as the counter-reactant. By using TBEA in the MLD growth scheme, a sulfur atom is incorporated into the backbone of the MLD reaction, without changing the reactivity of the alkylamine coupling moieties. The sulfur atom can be used as a tracer atom to measure both concentration and placement of the TBEA backbone within the MLD film. The XPS spectrum for a film completely replacing ED with TBEA is given in Figure 8. The film composition as measured by XPS had atomic ratios S/O/N/C of 1:3.0:4.1:14.7, which agrees well with the theoretical ratios of 1:2:4:12 for the pure PDIC/TBEA film. To create a blended film of PDIC/ED/TBEA, the dosing was alternated between ED and TBEA for each diamine dose. This should result in a film with close to half the concentration of sulfur of the pure PDIC/TBEA film,[59] with the sulfur atoms spread evenly throughout the film thickness. Indeed, from the XPS given in Figure 8, atomic ratios are 1:3.9:6.8:22.1 for S/O/N/C, which is close to the theoretical ratios of 1:4:8:22 for the 50% ED/50% TBEA film. Thus the film composition can be controlled by substituting TBEA for ED.

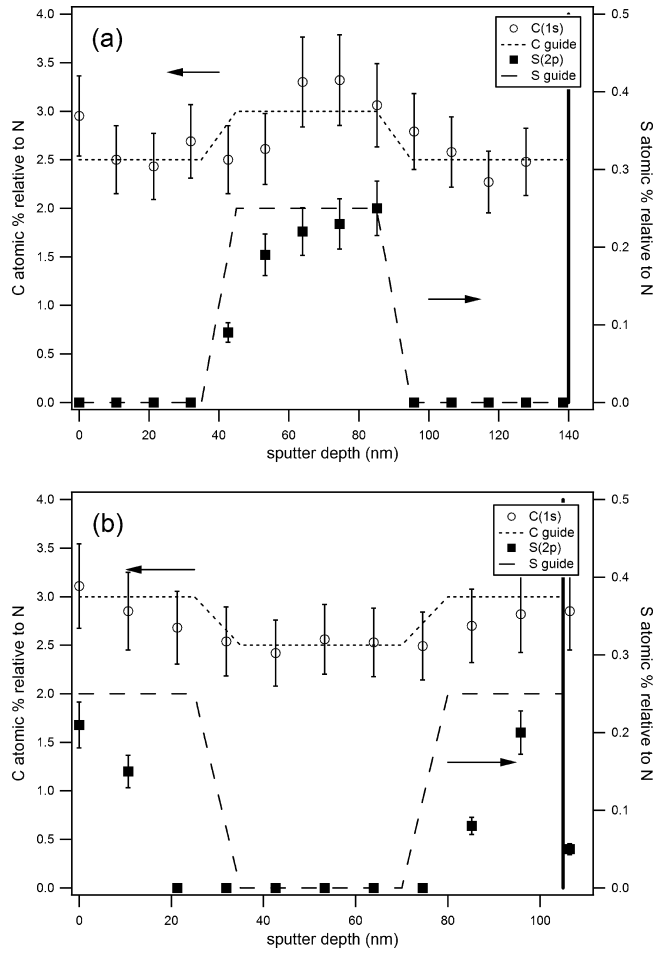

Figure 9. Depth profiles of laminate films for (a) laminate 1 with ED/TBEA/ED layering and (b) laminate 2 with TBEA/ED/TBEA layering. Theoretical film concentration is indicated by the dashed line. Error bars are based on instrumental uncertainties of the XPS system.

In addition to creating uniform films incorporating TBEA, the position of TBEA can be controlled in the film by alternating cycles to form blocks of PDIC/ED and blocks of PDIC/TBEA. By alternating blocks in this manner, nanolaminates can be formed by MLD, with discrete layers of chemically distinct films. To test the capability of forming nanolaminates by this MLD coupling chemistry, films were deposited with layers alternating between ED and TBEA chemistry, for 30−50 nm of film growth per layer. The layer thickness of 30−50 nm was chosen to be compatible with the depth resolution of the XPS sputter technique (avoiding signal crossover from the underlying layers); however, the nanolaminate technique should be applicable for much thinner layers as well.

In laminate 1, 40 nm PDIC/ED, followed by 50 nm of PDIC/TBEA, then another 40 nm PDIC/ED, was deposited to form a three-layer film. The sputter depth profile of the resulting film is given in Figure 9a. Figure 9 shows that around 40 nm into the film, the sulfur and carbon signals begin to increase,

due to the TBEA layer. At the interface with the PDIC/ED layer there is a transition region, where the sulfur signal increases rapidly. The mapping of this transition region is ambiguous, due to the film depth covered between sample points. A theoretical guide indicating a 10 nm transition region based on the minimum sampling depth resolution of the XPS system is provided to help direct the eye, but the experimental transition region may be as wide as 20 nm. The transition region is followed by a central region in which, rather than containing a constant concentration of sulfur as expected for the PDIC/TBEA layer, the signal increases slowly to the expected level. The bottom interface between the TBEA and ED layers is sharp, with the sulfur concentration decreasing rapidly from the theoretically expected value to zero, over a sputter depth of 85−95 nm. The slow increase of the sulfur signal with depth in the central region may indicate deficiencies in packing or possibly unreacted sites within the TBEA region, which would allow for penetration of ED into the central TBEA layer and lead to the observed effect. For the PDIC/ED layer, we expect a C/N ratio of 2.5 and a S/N ratio of 0, while for the PDIC/TBEA layer we expect a C/N ratio of 3 and a S/N ratio of 0.25. It is evident from Figure 9 that the measured film composition matches closely with the expected values for the film in each of the three layers.

In laminate 2, the films are deposited in the opposite order, with the first layer deposited as 30 nm of PDIC/TBEA, the second as 40 nm PDIC/ED, and the third layer 30 nm PDIC/TBEA. The depth profile for this laminate is given in Figure 9b and shows that, again, the sulfur and carbon track with the layers of the laminate. The sulfur composition peaks at the same maximum value for the first and third layers of the laminate, at a value close to the theoretical level, and drops to zero as expected for the PDIC/ED middle layer of the laminate. While the laminate layer thicknesses do not match identically with the theoretical line, the composition of each layer agrees well. The thickness discrepancy is attributed to an abnormally low growth rate for the PDIC/TBEA layers. This may have been caused by a reduced dose pressure for the TBEA resulting from a blockage in the dosing valve during this deposition. Even with the value in this case, it is interesting to note that the growth rate remains constant, as the chemically discrete TBEA/PDIC layers are observed to be of the same thickness. These laminates demonstrate the versatility of MLD, which allows for precise tuning of organic film composition, at specific locations within the film. While we have shown laminates with layer thicknesses of ~30 nm, the laminate layer thickness can be increased or decreased as desired, and should readily allow for thicknesses of 5 nm and below. In fact, when carried out to the limit of a single molecule thickness, the laminate is the blended film, with constant composition through the film. These laminates and blends should be important in future nanoscale devices in which subnanometer composition control of conformal organic thin films is desired.

CONCLUSION

We have successfully demonstrated the MLD growth of polyurea films using PDIC and ED as monomers. The deposition of these films occurs with a constant growth rate, and shows self-limiting saturation behavior in each of the reactants. TEM confirms the film thickness values measured by ellipsometry, and indicates that the films are highly uniform. FTIR spectra show strong absorption from amide modes, which are expected from the urea-coupling chemistry, while lacking the characteristic isocyanate stretching mode, indicating that reaction of the isocyanate is complete. Film composition is stoichiometric by XPS measurements, with three distinct carbon species, as expected. The films demonstrate excellent stability in both ambient lab conditions and at elevated temperatures under vacuum. The growth rate decreases with increasing temperature, suggesting a precursor-mediated reaction mechanism.

The film composition was varied at the nanoscale by substituting cycles of ED in the MLD scheme with TBEA. In this way, nanolaminates were created, using alternating layers of PDIC/ED and PDIC/TBEA, with layer thicknesses of 30−50 nm. This thickness can be decreased as desired, to the limit of molecular laminates. By changing the diamine precursor molecule between ED and TBEA for every other cycle, a uniformly blended film is created, with constant composition through the film thickness. The ability to control the film composition at the molecular level is a major benefit of using MLD. Not only can the total film composition be controlled, but the thickness of films can be controlled, so that nanoscale films can be created with desired compositions, including nanolaminates. Growth of polyurea films by MLD, as demonstrated here, offers access to ultrathin, conformal organic coatings. The molecular level control delivered by the process can be applied to the field of electronic materials, where control of film properties on the nanoscale is essential. The true versatility of MLD results in the ability to tailor-make organic films for individual applications. Initial functionalization of the surface to yield a reactive chemical moiety can be achieved by different methods, which can then be followed by deposition of an organic film by MLD, with desired properties selected by choice of specific monomers. The organic film can be capped with a different chemical functionality, by changing the final monomer at-

tached to a heterobifunctional molecule that includes the desired terminus. With the ability to design diverse nanoscale organic thin films with molecular control, we expect that MLD chemistries will continue to find new and novel applications in a wide range of fields.

METHODS

Description of Materials and Reactor. MLD films were deposited in a hot wall reactor, pumped by a Leybold Trivac rotary vane pump. The reactor was heated by external heating tapes controlled by a variable transformer. The base pressure of the reactor was below 1 mtorr, with pressure measured by a Lesker convection gauge. MLD monomers and nitrogen purge gas were introduced into the reactor from a source manifold using solenoid valves controlled by LabVIEW.

3-Aminopropyltriethoxysilane (APTES), ethylenediamine (ED), and 1,4-phenylene diiscocyanate (PDIC) were purchased from Sigma Aldrich, and 2,2′-thiobis(ethylamine) (TBEA) was purchased from TCI America, with all reagents used as received. Films were deposited on (100) silicon wafers with a 4 nm thermal oxide.

Initial Surface Functionalization. Silicon dioxide samples were cleaned for 15 min in a fresh piranha cleaning solution with 7:3 ratio of 98% sulfuric acid/30% hydrogen peroxide, then rinsed in deionized water (Caution: Fresh piranha solution is hot and extremely corrosive. Proper training and extreme care should be taken when handling piranha solution.) Following sample drying by compressed air, the samples were loaded into the MLD reactor and the temperature was ramped to 100 °C and held at this temperature for 30 min. After the heat treatment, APTES was dosed into the chamber from a liquid vial submerged in a bath of 45 °C water, which was used to increase the vapor pressure of APTES introduced into the reactor. As APTES was dosed into the reactor, the reactor was closed off from the pump for the dose of 60 min. The chamber was then evacuated while flowing a small pressure of nitrogen to aid pumping and to prevent backstreaming from the pump. Following evacuation, the heating was turned off.

Molecular Layer Deposition. Each complete binary MLD cycle involves a PDIC dose, followed by purging with nitrogen, then an ED dose, followed by another nitrogen purge. PDIC is a solid below 96 °C, so to improve the dosing pressure, the vial containing PDIC was heated in a silicone oil bath held at 50 °C. This temperature was chosen as it was the highest temperature that did not lead to bulk sublimation and recondensation of the solid PDIC onto the vial and valve above the oil bath.

Following APTES treatment, MLD dosing began once the chamber reached the desired growth temperature. For the room temperature case, dosing began once the chamber reached a temperature of 35 °C, and the chamber continued to cool toward room temperature during the remainder of the MLD process. Since no fluctuations in the growth rate were observed during this period it appears that having the initial doses occur at a slightly higher substrate temperature did not affect the initial growth rate relative to that of the subsequent doses at room temperature. The dosing procedure was to open the valve to the PDIC vial while isolating the reactor from the pump, to allow for a batch process. The PDIC dose was followed by a nitrogen purge to remove residual PDIC vapor. ED is a liquid with a high vapor pressure (10 mmHg at 20 °C), so it was kept at room temperature. ED was dosed by isolating the reactor from the pump and leaking in ED until a pressure of 3 Torr was reached. This pressure was held for the duration of the dose time. The ED dose was also followed by a nitrogen purge step, which completed one MLD binary cycle. Saturation and temperature dependent growth rates were calculated from the film thickness measured after 20 MLD cycles.

For experiments using TBEA, the TBEA dose replaced the ED dose in a specific cycle. TBEA is liquid at room temperature, with a lower vapor pressure than that of ED (~300 mmHg at 20 °C), and thus the dose time was modified. Like ED, TBEA was dosed by isolating the reactor from the pump, but for TBEA the dose pressure was limited to 200 mtorr. Samples were exposed to different numbers of MLD cycles in individual experiments—each experiment ended once the chamber was opened to atmosphere. Following MLD, samples were removed from the reactor for *ex situ* analysis.

Characterization Techniques. Ellipsometry measurements were performed on a Gaertner L116C ellipsometer using a 70° angle of incidence and the polarizer set to 45°, with 632.8 nm light. The instrument software calculated the ellipsometric angles Δ and Ψ, and iteratively solved for film thickness values. To test film uniformity across a sample, the sample thickness was measured in no fewer than 3 different locations on the sample. Owing to the similarity in the index of refraction for SiO_2 and that of the organic film,[46,47,50] a single film thickness was determined, as a solution could not be found for a double-layer film model. The single index of refraction used for the SiO_2 and combined film was $n_f = 1.46$. For each experiment, the silicon dioxide thickness of piranha-cleaned silicon samples was measured, and this value was used as a baseline oxide thickness, which was subtracted from the subsequent total film thickness values to yield the thickness of the deposited organic film.

X-ray photoelectron spectroscopy (XPS) was performed on a Surface Science Instruments S-Probe spectrometer. The excitation source was Al Kα radiation, which has an energy of 1486.6 eV. Survey scans used an energy step of 1 eV, while fine scans used an energy step of 0.1 eV. Atomic percentages were calculated by finding peak integrals, and peaks were fit using pure Gaussian profiles with a Shirley background. Multiple peaks within a single fine scan were fit while constraining the peak widths from the different species to be identical. Depth profiling was performed on a Phyiscal Electronics, Inc. 5000 Versaprobe XPS using an excitation source of Al Kα radiation. The samples were sputtered using a Physical Electronics, Inc. C_{60} sputter gun, with a sputter current of 20 nA at 10 kV, and a sputter area of 2 mm $\times$ 2 mm. An electron charge neutralizer at 30 eV was used to prevent charging during sputter experiments.

FTIR measurements were made in a transmission geometry on a Thermo Nicolet 6700 FT-IR spectrometer using a MCT-A detector. Spectra were taken with 200 scans, at 4 cm^{-1} resolution. Piranha-cleaned samples were used as a background reference unless otherwise specified. Water and carbon-dioxide peaks have been subtracted as necessary during the baselining process.

The high resolution TEM image was acquired using a 200 kV TEM from a specimen prepared using conventional 30 keV FIB milling *via* the *in situ* lift-out technique. To enable visualization of the organic film, the samples were first coated with a 100 nm layer of evaporated Cu.

Density functional theory calculations were performed using the Gaussian 03 software suite.[60] All calculations were performed using the B3LYP functional[61,62] with the 6-311++G** basis set. Optimizations were performed without constraints on any atoms, and vibrational frequencies were calculated for the expected products, to simulate IR absorption spectra. All simulated IR absorption spectra have frequencies scaled by a factor of 0.9614.[63]

Acknowledgment. We would like to acknowledge support of this work from the National Science Foundation (CHE 0615087) and the Semiconductor Research Corporation *via* the Center for Advanced Interconnect Science and Technology (SRC task 1292.040). We would also like to thank C. Hitzman for helpful discussions regarding XPS depth profiling experiments.

Supporting Information Available: Complete ref 60 and thermal annealing FTIR spectra. This material is available free of charge *via* the Internet at http://pubs.acs.org.

REFERENCES AND NOTES

1. Braga, D.; Horowitz, G. High-Performance Organic Field-Effect Transistors. *Adv. Mater.* **2009**, *21*, 1473–1486.
2. DiBenedetto, S. A.; Facchetti, A.; Ratner, M. A.; Marks, T. J. Molecular Self-Assembled Monolayers and Multilayers for Organic and Unconventional Inorganic Thin-Film Transistor Applications. *Adv. Mater.* **2009**, *21*, 1407–1433.
3. Hill, I. G.; Weinert, C. M.; Kreplak, L.; van Zyl, B. P. Influence of Self-Assembled Monolayer Chain Length on Modified Gate Dielectric Pentacene Thin-Film Transistors. *Appl. Phys. A* **2009**, *95*, 81–87.
4. Ito, Y.; Virkar, A. A.; Mannsfeld, S.; Joon, H. O.; Toney, M.; Locklin, J.; Bao, Z. Crystalline Ultrasmooth Self-Assembled Monolayers of Alkylsilanes for Organic Field-Effect Transistors. *J. Am. Chem. Soc.* **2009**, *131*, 9396–9404.
5. Mottaghi, M.; Lang, P.; Rodriguez, F.; Rumyantseva, A.; Yassar, A.; Horowitz, G.; Lenfant, S.; Tondelier, D.; Vuillaume, D. Low-Operating-Voltage Organic Transistors Made of Bifunctional Self-Assembled Monolayers. *Adv. Funct. Mater.* **2007**, *17*, 597–604.
6. Tulevski, G. S.; Miao, Q.; Fukuto, M.; Abram, R.; Ocko, B.; Pindak, R.; Steigerwald, M. L.; Kagan, C. R.; Nuckolls, C. Attaching Organic Semiconductors to Gate Oxides: *In Situ* Assembly of Monolayer Field Effect Transistors. *J. Am. Chem. Soc.* **2004**, *126*, 15048–15050.
7. Roberts, M. E.; Sokolov, A. N.; Bao, Z. Material and Device Considerations for Organic Thin-Film Transistor Sensors. *J. Mater. Chem.* **2009**, *19*, 3351–3363.
8. Ashwell, G. J.; Wierzchowiec, P.; Phillips, L. J.; Collins, C. J.; Gigon, J.; Robinson, B. J.; Finch, C. M.; Grace, I. R.; Lambert, C. J.; Buckle, P. D.; *et al.* Functional Molecular Wires. *Phys. Chem. Chem. Phys.* **2008**, *10*, 1859–1866.
9. Aswal, D. K.; Lenfant, S.; Guerin, D.; Yakhmi, J. V.; Vuillaume, D. Self-Assembled Monolayers on Silicon for Molecular Electronics. *Anal. Chim. Acta* **2006**, *568*, 84–108.
10. Wheeler, W. D.; Dahnovsky, Y. Molecular Transistors with Perpendicular Gate Field Architecture: A Strong Gate Field Effect. *J. Phys. Chem. C* **2009**, *113*, 1088–1092.
11. Murthy, B. R.; Yee, W. M.; Krishnamoorthy, A.; Kumar, R.; Frye, D. C. Self-Assembled Monolayers as Cu Diffusion Barriers for Ultralow-*k* dielectrics. *Electrochem. Solid-State Lett.* **2006**, *9*, F61–F63.
12. Gandhi, D. D.; Ganesan, P. G.; Chandrasekar, V.; Gan, Z.; Mhaisalkar, S. G.; Li, H.; Ramanath, G. Molecular-Nanolayer-Induced Suppression of in-Plane Cu Transport at Cu−Silica Interfaces. *Appl. Phys. Lett.* **2007**, *90*, 163507.
13. Gandhi, D. D.; Lane, M.; Zhou, Y.; Singh, A. P.; Nayak, S.; Tisch, U.; Eizenberg, M.; Ramanath, G. Annealing-Induced Interfacial Toughening Using a Molecular Nanolayer. *Nature* **2007**, *447*, 299–302.
14. Gandhi, D. D.; Tisch, U.; Singh, B.; Eizenberg, M.; Ramanath, G. Ultraviolet-Oxidized Mercaptan-Terminated Organosilane Nanolayers as Diffusion Barriers at Cu−Silica Interfaces. *Appl. Phys. Lett.* **2007**, *91*, 143503.
15. Yoshino, T.; Hata, N.; Muramoto, I.; Machida, H.; Kikkawal, T. Effect of Phosphorus Atom in Self-Assembled Monolayer as a Drift Barrier for Advanced Copper Interconnects. *Appl. Phys. Exp.* **2008**, *1*, 065003.
16. Ritala, M.; Leskela, M., Atomic Layer Deposition. In *Handbook of Thin Film Materials*; Nalwa, H. S., Ed.; Academic Press: San Diego, CA, 2002; Vol. 1.
17. Bitzer, T.; Richardson, N. V. Demonstration of an Imide Coupling Reaction on a Si(100)-2 × 1 Surface by Molecular Layer Deposition. *Appl. Phys. Lett.* **1997**, *71*, 662–664.
18. Bitzer, T.; Richardson, N. V. Route for Controlled Growth of Ultrathin Polyimide Films with Si−C Bonding to Si(100)-2 × 1. *Appl. Surf. Sci.* **1999**, *145*, 339–343.
19. Yoshimura, T.; Tatsuura, S.; Sotoyama, W. Polymer Films Formed with Monolayer Growth Steps by Molecular Layer Deposition. *Appl. Phys. Lett.* **1991**, *59*, 482–484.
20. Adamczyk, N. M.; Dameron, A. A.; George, S. M. Molecular Layer Deposition of Poly(*p*-phenylene terephthalamide) Films Using Terephthaloyl Chloride and *p*-Phenylenediamine. *Langmuir* **2008**, *24*, 2081–2089.
21. Du, Y.; George, S. M. Molecular Layer Deposition of Nylon 66 Films Examined Using *in situ* FTIR Spectroscopy. *J. Phys. Chem. C* **2007**, *111*, 8509–8517.
22. Shao, H.-L.; Umemoto, S.; Kikutani, T.; Okui, N. Layer-by-Layer Polycondensation of Nylon 66 by Alternating Vapour Deposition Polymerization. *Polymer* **1997**, *38*, 459–462.
23. Kim, A.; Filler, M. A.; Kim, S.; Bent, S. F. Layer-by-Layer Growth on Ge(100) *via* Spontaneous Urea Coupling Reactions. *J. Am. Chem. Soc.* **2005**, *127*, 6123–6132.
24. Usui, H. Polymeric Film Deposition by Ionization-Assisted Method for Optical and Optoelectronic Applications. *Thin Solid Films* **2000**, *365*, 22–29.
25. George, S. M.; Yoon, B.; Dameron, A. A. Surface Chemistry for Molecular Layer Deposition of Organic and Hybrid Organic−Inorganic Polymers. *Acc. Chem. Res.* **2009**, *42*, 498–508.
26. Lee, J. S.; Lee, Y. J.; Tae, E. L.; Park, Y. S.; Yoon, K. B. Synthesis of Zeolite as Ordered Multicrystal Arrays. *Science* **2003**, *301*, 818–821.
27. Yoshimura, T.; Kudo, Y. Monomolecular-Step Polymer Wire Growth from Seed Core Molecules by the Carrier-Gas-Type Molecular Layer Deposition. *Appl. Phys. Exp.* **2009**, *2*, 015502.
28. Dameron, A. A.; Seghete, D.; Burton, B. B.; Davidson, S. D.; Cavanagh, A. S.; Bertrand, J. A.; George, S. A. Molecular Layer Deposition of Alucone Polymer Films Using Trimethylaluminum and Ethylene Glycol. *Chem. Mater.* **2008**, *20*, 3315–3326.
29. Lee, B. H.; Im, K. K.; Lee, K. H.; Im, S.; Sung, M. M. Molecular Layer Deposition of ZrO_2-Based Organic−Inorganic Nanohybrid Thin Films for Organic Thin Film Transistors. *Thin Solid Films* **2009**, *517*, 4056–4060.
30. Peng, Q.; Gong, B.; VanGundy, R. M.; Parsons, G. N. "Zincone" Zinc Oxide−Organic Hybrid Polymer Thin Films Formed by Molecular Layer Deposition. *Chem. Mater.* **2009**, *21*, 820–830.
31. Yoon, B.; O'Patchen, J. L.; Seghete, D.; Cavanagh, A. S.; George, S. M. Molecular Layer Deposition of Hybrid Organic−Inorganic Polymer Films Using Diethylzinc and Ethylene Glycol. *Chem. Vap. Deposition* **2009**, *15*, 112–121.
32. Dolbier, W. R.; Beach, W. F. Parylene-AF4: A Polymer With Exceptional Dielectric and Thermal Properties. *J. Fluorine Chem.* **2003**, *122*, 97–104.
33. Rogojevic, S.; Moore, J. A.; Gill, W. N. Modeling Vapor Deposition of Low-κ Polymers: Parylene and Polynaphthalene. *J. Vac. Sci. Technol., A* **1999**, *17*, 266–274.
34. Senkevich, J. J.; Wang, P. I. Molecular Layer Chemistry *via* Parylenes. *Chem. Vap. Deposition* **2009**, *15*, 91–94.
35. Baxamusa, S. H.; Im, S. G.; Gleason, K. K. Initiated and Oxidative Chemical Vapor Deposition: A Scalable Method for Conformal and Functional Polymer Films on Real Substrates. *Phys. Chem. Chem. Phys.* **2009**, *11*, 5227–5240.
36. Tenhaeff, W. E.; Gleason, K. K. Initiated and Oxidative Chemical Vapor Deposition of Polymeric Thin Films: iCVD and oCVD. *Adv. Funct. Mater.* **2008**, *18*, 979–992.
37. Takahashi, Y.; Ukishima, S.; Iijima, M.; Fukada, E. Piezoelectric Properties of Thin-Films of Aromatic Polyurea Prepared by Vapor-Deposition Polymerization. *J. Appl. Phys.* **1991**, *70*, 6983–6987.
38. Wang, X. S.; Takahashi, Y.; Iijima, M.; Fukada, E. Piezoelectric and Dielectric Properties of Aromatic Polyureas Synthesized by Vapor Deposition Polymerization. *Jpn. J. Appl. Phys.* **1995**, *34*, 1585–1590.
39. Hattori, T.; Iijima, M.; Takahashi, Y.; Fukada, E.; Suzuki, Y.; Kakimoto, M.; Imai, Y. Synthesis of Aliphatic Polyurea Films by Vapor-Deposition Polymerization and Their Piezoelectric Properties. *Jpn. J. Appl. Phys.* **1994**, *33*, 4647–4651.
40. Tsukiji, M.; Kowa, H.; Muraki, K.; Umeda, N.; Morii, K.; Honda, M.; Tajitsu, Y. Accurate Measurement of Light Modulation Properties of Piezoelectric Polymer. *Jpn. J. Appl. Phys.* **2006**, *45*, 7531–7534.
41. Hattori, T.; Takahashi, Y.; Iijima, M.; Fukada, E. Piezoelectric and Ferroelectric Properties of Polyurea-5 Thin Films

Prepared by Vapor Deposition Polymerization. *J. Appl. Phys.* **1996**, *79*, 1713–1721.
42. Wang, X. S.; Iijima, M.; Takahashi, Y.; Fukada, E. Dependence of Piezoelectric and Pyroelectric Activities of Aromatic Polyurea Thin-Films on Monomer Composition Ratio. *Jpn. J. Appl. Phys.* **1993**, *32*, 2768–2773.
43. Tajitsu, Y.; Ohigashi, H.; Hirooka, A.; Yamagishi, A.; Date, M.; Hattori, T.; Fukada, E. Ferroelectric Behavior in Thin Films of Polyurea-5. *Jpn. J. Appl. Phys.* **1996**, *35*, 5199–5202.
44. Ek, S.; Iiskola, E. I.; Niinisto, L. Gas-Phase Deposition of Aminopropylalkoxysilanes on Porous Silica. *Langmuir* **2003**, *19*, 3461–3471.
45. Cai, C.-J.; Shen, Z.-G.; Xing, Y.-S.; Ma, S.-L. Surface Topography and Character of γ-Aminopropyltriethoxysilane and Dodecyltrimethoxysilane Films Adsorbed on the Silicon Dioxide Substrate *via* Vapour Phase Deposition. *J. Phys. D: Appl. Phys.* **2006**, *39*, 4829–4837.
46. Haller, I. Covalently Attached Organic Monolayers on Semiconductor Surfaces. *J. Am. Chem. Soc.* **1978**, *100*, 8050–8055.
47. Howarter, J. A.; Youngblood, J. P. Optimization of Silica Silanization by 3-Aminopropyltriethoxysilane. *Langmuir* **2006**, *22*, 11142–11147.
48. Simon, A.; Cohen-Bouhacina, T.; Porte, M. C.; Aime, J. P.; Baquey, C. Study of Two Grafting Methods for Obtaining a 3-Aminopropyltriethoxysilane Monolayer on Silica Surface. *J. Colloid Interface Sci.* **2002**, *251*, 278–283.
49. Toworfe, G. K.; Composto, R. J.; Shapiro, I. M.; Ducheyne, P. Nucleation and Growth of Calcium Phosphate on Amine-, Carboxyl-, and Hydroxyl-Silane Self-Assembled Monolayers. *Biomaterials* **2006**, *27*, 631–642.
50. Vandenberg, E. T.; Bertilsson, L.; Liedberg, B.; Uvdal, K.; Erlandsson, R.; Elwing, H.; Lundstroem, I. Structure of 3-Aminopropyl Triethoxy Silane on Silicon Oxide. *J. Colloid Interface Sci.* **1991**, *147*, 103–118.
51. Pasternack, R. M.; Amy, S. R.; Chabal, Y. J. Attachment of 3-(Aminopropyl)triethoxysilane on Silicon Oxide Surfaces: Dependence on Solution Temperature. *Langmuir* **2008**, *24*, 12963–12971.
52. Zheng, W.; Frank, C. W., Surface-initiated Vapor Deposition Polymerization of Poly(γ-benzyl-L-glutamate): Optimization and Mechanistic Studies. Langmuir, In press.
53. Kurth, D. G.; Bein, T. Surface Reactions on Thin Layers of Silane Coupling Agents. *Langmuir* **1993**, *9*, 2965–2973.
54. This linear dependence supports the validity of our room temperature dosing procedure, in which the MLD process takes place while the chamber cools from 45 °C to room temperature, since no effect on the linearity of the MLD growth is observed.
55. The region of darker contrast in the MLD layer on the Cu side of the film suggests that Cu migrated several nanometers into the organic layer.
56. Coleman, M. M.; Sobkowiak, M.; Pehlert, G. J.; Painter, P. C.; Iqbal, T. Infrared Temperature Studies of a Simple Polyurea. *Macromol. Chem. Phys.* **1997**, *198*, 117–136.
57. Raunier, S.; Chiavassa, T.; Marinelli, F.; Aycard, J. P. Experimental and Theoretical Study on the Spontaneous Formation of OCN^-: Reactivity between HNCO and NH_3/H_2O Environment at Low Temperature. *Chem. Phys.* **2004**, *302*, 259–264.
58. FTIR spectra for thermal annealing are available in Supporting Information.
59. The film composition will not be exactly half that of the PDIC/TBEA film, since the substitution of TBEA with ED introduces a higher content of carbon into the film as well. Thus the 1:1 blend of ED/TBEA has a sulfur composition that is 54% the sulfur composition in the pure TBEA film.
60. Frisch, M. J.; Trucks, G. W.; Schlegel, H. B.; Scuseria, G. E.; Robb, M. A.; Cheeseman, J. R.; Montgomery, J., J. A.; Vreven, T.; Kudin, K. N.; Burant, J. C.; *et al*. *Gaussian 03*, revision D.01; Gaussian, Inc.: Wallingford, CT, 2004.
61. Becke, A. D., III. The Role of Exact Exchange. *J. Chem. Phys.* **1993**, *98*, 5648–5652.
62. Lee, C. T.; Yang, W. T.; Parr, R. G. Development of the Colle−Salvetti Correlation-Energy Formula Into a Functional of the Electron-Density. *Phys. Rev. B* **1988**, *37*, 785–789.
63. Scott, A. P.; Radom, L. Harmonic Vibrational Frequencies: An Evaluation of Hartree−Fock, Møller−Plesset, Quadratic Configuration Interaction, Density Functional Theory, and Semiempirical Scale Factors. *J. Phys. Chem.* **1996**, *100*, 16502–16513.